Dopplerfree spectrum of the B 1Π–X 1Σ+ transition of NaK, and the perturbation and hyperfine splitting

Masaaki Baba, Shinji Tanaka, and Hajime Katô

Citation: The Journal of Chemical Physics **89**, 7049 (1988); doi: 10.1063/1.455334
View online: http://dx.doi.org/10.1063/1.455334
View Table of Contents: http://scitation.aip.org/content/aip/journal/jcp/89/12?ver=pdfcov
Published by the AIP Publishing

Doppler-free spectrum of the $B\,^1\Pi$–$X\,^1\Sigma^+$ transition of NaK, and the perturbation and hyperfine splitting

Masaaki Baba, Shinji Tanaka, and Hajime Katô
Department of Chemistry, Faculty of Science, Kobe University, Nada-ku, Kobe 657, Japan

(Received 5 July 1988; accepted 6 September 1988)

The Doppler-free high-resolution spectrum of the $B\,^1\Pi$–$X\,^1\Sigma^+$ transition of NaK was measured by the technique of laser polarization spectroscopy. The molecular constants of the $B\,^1\Pi$ state, which reproduced the observed 831 unperturbed line positions ($v = 0$–6, $J = 1$–94) with a standard deviation of 0.002 cm^{-1}, were determined. Many perturbed lines, which were attributed to the perturbation between the $B\,^1\Pi$ and $c(2)\,^3\Sigma^+$ states, were observed. By analyzing the energy shifts of the $B\,^1\Pi(v = 4,J)$ levels around $J = 13$, we estimated the rotational constant B_v of the $c(2)\,^3\Sigma^+$ state to be 0.048 cm^{-1}, and the matrix element of the spin-orbit interaction $\langle c(2)\,^3\Sigma^+ vN = JJM|H_{so}|B\,^1\Pi v = 4JM\rangle$ to be 0.14 cm^{-1}. We found that the strongly perturbed lines split into four lines, and we identified them as a hyperfine splitting caused by a mixing of the $c(2)\,^3\Sigma^+$ state. The splitting into four lines is explained by the magnetic dipole interaction due to a nucleus of $I = 3/2$.

I. INTRODUCTION

Since the pioneering spectroscopic study on the NaK molecule was done by Loomis *et al.* in 1930,[1] a number of spectroscopic experiments[2–9] and theoretical calculations[10–14] have been reported. The fluorescence to the $a(1)\,^3\Sigma^+$ state was observed when the NaK molecule was excited to the $D(2)\,^1\Pi$ state.[15] It was shown that this fluorescence was due to the mixing of the $D(2)\,^1\Pi$ state and the closely located $d(2)\,^3\Pi$ state.[15–19] The perturbation of the $B\,^1\Pi$ state was found by Breford *et al.*[20] They observed the fluorescence to the $a(1)\,^3\Sigma^+$ state, and the perturbing state was suggested to be the $b(1)\,^3\Pi$ state.

Recently, Derouard *et al.*[21] studied the energy shifts of many perturbed lines of the $B\,^1\Pi$ state using *e–f* Stark mixing spectroscopy. They identified the perturbing state to be the $c(2)\,^3\Sigma^+$ state. The identification was deduced from (i) the observation of the fluorescence to the $a(1)\,^3\Sigma^+$ state which consists of a series of doublets for both *e* and *f* type excited levels, and (ii) the selection rules of perturbed levels of the $B\,^1\Pi$ state deduced from the measurement of the energy shifts. Barrow *et al.*[22] obtained the molecular constants of the $B\,^1\Pi$ state by analyzing the laser-induced fluorescence spectra detected by a Fourier-transform spectrometer, and the dye-laser excitation spectra. Fourier-transform spectroscopy provides information of high precision, but their study covered only a small number of the v, J levels in the $B\,^1\Pi$ state. Many levels of the $B\,^1\Pi$ state were observed by excitation spectroscopy.

We have observed the Doppler-free high-resolution spectrum of the $B\,^1\Pi$–$X\,^1\Sigma^+$ transition with an accuracy of $\pm$ 100 MHz using the technique of laser polarization spectroscopy,[23] and the results shall be reported in this article. The molecular constants G_v, B_v, D_v, and H_v of the $B\,^1\Pi$ state for each vibrational level of $v = 0$–6 shall be determined with high accuracy by using a nonlinear least-squares fitting procedure.[24] By analyzing the energy shifts of the perturbed levels, we shall estimate the rotational constant B_v of the $c(2)\,^3\Sigma^+$ state and the matrix element of the spin–orbit interaction. We found that the strongly perturbed lines split into four lines, and we shall discuss the origin of the splitting.

II. EXPERIMENTAL

Experimental details of the laser polarization spectroscopy have been described elsewhere.[25] We used a single mode ring dye laser equipped with the autoscan system (Coherent 699-29, linewidth 500 kHz, at the output of Rhodamine 6G). NaK was obtained in a heat pipe oven operated at 400 °C with Ar as the buffer gas at 1.5 Torr. We used potassium metal which contains about 0.1% of sodium as an impurity. The linewidth of the rotational line of NaK was nominally about 100 MHz under this condition. We simultaneously recorded the fluorescence excitation spectrum of iodine and calibrated the absolute wavelength of the scanning laser to an accuracy of $\pm$ 100 MHz.

A fluorescence spectrum was observed by tuning the laser light to a specific rotational line. Fluorescence in the heat pipe oven was dispersed by a monochromator (Spex 1269) and detected with a photon counting system (EG&G PARC Model 1109) with a photomultiplier (RCA C31034).[26] The spectral resolution was about 1 cm^{-1} in the measurements.

III. RESULTS AND DISCUSSION

A part of the Doppler-free polarization spectrum is shown in Fig. 1, which contains the rotational lines of the $B\,^1\Pi(v' = 4)$–$X\,^1\Sigma^+(v'' = 1)$ transition. When circularly polarized light is used as the pump beam, P and R lines can be observed in the polarization spectrum (Fig.1 upper trace). In practice, Q lines appear in the spectrum with the dispersion shape because of the imperfect polarization of the optical system. On the other hand, when linearly polarized light is used as the pump beam, Q lines can be observed with high intensity (Fig.1 lower trace). Thus, we can easily distinguish the Q line. The vibrational and rotational quantum numbers of about 900 spectral lines of the $B\,^1\Pi(v' = 0$–$6)$–$X\,^1\Sigma^+$ transitions were assigned. A number of these lines

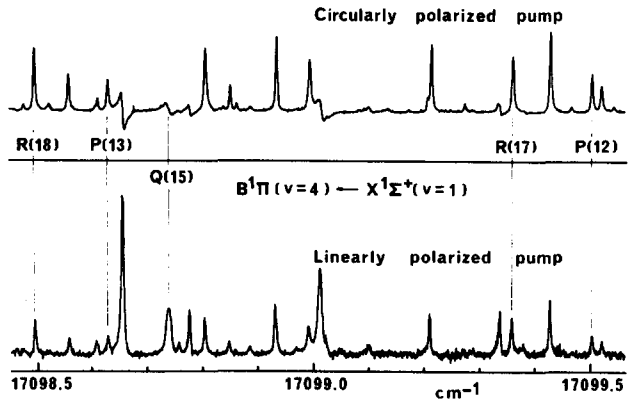

FIG. 1. A part of the laser polarization spectrum of NaK around the $B\,^1\Pi(v'=4,J'=15)$–$X\,^1\Sigma^+(v''=1,J''=15)$ transition; $Q(15)$. Upper trace: pumped by circularly polarized light; lower trace: pumped by linearly polarized light.

were found to be perturbed, and 832 unperturbed lines were used to determine the molecular constants. Table I gives the distribution of the spectral lines.[27]

We have adopted the molecular constants of the $X\,^1\Sigma^+$ state reported by Ross *et al.*[28] Molecular constants G_v, B_v, D_v, H_v, and Λ-doubling constants of the $B\,^1\Pi$ state were determined by using a nonlinear least-squares fitting procedure,[24] and the results are listed in Table II. These separate fits are taken together as input data for least-squares fits which yield the Dunham coefficients Y_{ij}. The molecular constants thus determined are listed in Table III. These constants reproduce the observed 831 unperturbed line positions of the $B\,^1\Pi(v'=0$–$6,\ J'=1$–$94)$–$X\,^1\Sigma^+$ transition with a standard deviation of 0.002 cm^{-1}. The molecular constants reported by Barrow *et al.*[22] are in good agreement with the present results. Since we observed a large number of spectral lines of the $B\,^1\Pi$ state with high accuracy, we could obtain more accurate values. We determined the equilibrium internuclear distance of the $B\,^1\Pi$ state to be 4.0138 Å, which is a little smaller than 4.016 Å obtained by Barrow *et al.* Our data are limited to low vibrational levels ($v=0$–6) of the $B\,^1\Pi$ state, while Barrow's data contain $v=0$–14. Hence, the molecular constants determined by Barrow *et al.* will be more accurate at high vibrational levels. From the molecular constants obtained above, the rotationless potential curve of the $B\,^1\Pi$ state was constructed up to the vibrational level of $v=6$ by the Rydberg–Klein–Rees (RKR) method,[29,30] and the results are listed in Table IV.

Let us now discuss the perturbed lines. We found irregularities of the spacing and intensity for many lines. An example of these perturbations is located around the $B\,^1\Pi(v'=4,J'=13)$ level, and it was confirmed by measuring both the $B\,^1\Pi(v'=4)$–$X\,^1\Sigma^+(v''=0)$ and $B\,^1\Pi(v'=4)$–$X\,^1\Sigma^+(v''=1)$ transitions. The difference between the measured and interpolated line positions (calculated from the molecular constants in Table II) is shown in Fig. 2. The largest energy shift was observed at $J'=13$ in the P and R lines. The level of $J'=13$ is shifted to the blue, and $J'=12$ to the red. For the Q lines, we observed large energy shifts in a pair of lines at $J'=11$ and 15. Similar shifts were observed by Derouard *et al.*[21] They also observed the fluorescence to the $a(1)\,^3\Sigma^+$ state following excitation to the strongly perturbed levels, and found that the fluorescence consists of a series of doublets for both e and f-type excited levels. From these results, they identified the perturbing state as $c(2)\,^3\Sigma^+$. We tuned the laser wavelength to the $Q(15)$ line of the $B\,^1\Pi(v'=4)$–$X\,^1\Sigma^+(v''=0)$ transition, and observed the fluorescence spectrum. A part of the transition to the $a(1)\,^3\Sigma^+$ state is shown in Fig. 4. The spectrum consists of sharp lines of bound–bound fluorescence (12 050–12 180 cm^{-1}) and a broad component of bound–continuum fluorescence (12 050–11 400 cm^{-1}). We also measured the fluorescence spectrum by exciting the $P(14)$ line of the $B\,^1\Pi(v'=4)$–$X\,^1\Sigma^+(v''=0)$ transition, and obtained a spectrum similar to Fig. 4. The sharp lines were composed of doublets for both P and Q line excitations.

TABLE I. Distribution of the spectral lines of the $B\,^1\Pi(v',J')$–$X\,^1\Sigma^+(v'',J'')$ transition, which were used to determine the molecular constants.

v'–v''	Spectral lines
0–4	R(69–88), Q(66–88), P(64–85)
0–5	R(0–16,18–22,24–36,38–56), Q(18–22,24–25,27–45,47–50), P(3–50)
1–1	R(69–76), Q(66–67,69–70,72–73), P(63–70)
1–2	R(2–25), Q(6–9,12–22), P(9,11–19)
1–4	R(87–93), Q(84–89,91,93–94), P(81–94)
2–0	R(3–9,11–12,14–17,19–24), Q(10–14,16–21), P(10–18)
2–2	R(48–58), Q(44–49,51–55), P(42–53)
2–6	R(4,6–9,11–22,24–25,27,31–34,36–58), Q(7–12,14–21,23–28,31, 34–35,37,39–43), P(6–19,21,25,27–28,30–37,39,41–49,51–52)
3–0	R(2,4,6–25,49–54), Q(3,5–19,21–24,46–48,50–52), P(3–4,6–20,44–50)
3–2	R(69–75), Q(65–72),P(63–67,69–70)
4–0	R(0–4,17–25,49–54,67–70), Q(2–7,22–25,45–48,51,66–68) P(3–7,20,22,43–49,63–66)
4–1	R(0–5,17–25), Q(1–6,21–23), P(2–3,5–7,20)
5–0	R(47–52,64–66,68–69), Q(45–50,62–63,66–67), P(44–48,60,64–65)
5–1	R(2–17,20–22,24,46–52), Q(10–21,45–47), P(3–19,44–47)
6–0	R(63–66,76–78), Q(61–64,75–77), P(60–63)
6–1	R(63–66),Q(61–64),P(59–61)
6–2	R(5–6,8–10,12–15,17–20), Q(5–9,11–17), P(3–4,6–7,9–12,14–15)

TABLE II. Molecular constants G_v, B_v, D_v, H_v, and Λ-doubling constants of the $B\,^1\Pi$ state. All values are in cm^{-1}.

v	G_v	$10^2 B_v$	$10^7 D_v$	$10^{12} H_v$	Λ doubling
0	35.4022	7.178 457	3.033 38	−1.116 49	-2.010×10^{-6}
1	104.5441	7.058 978	3.156 20	−1.424 50	-2.081×10^{-6}
2	171.3055	6.936 274	3.321 19	−1.343 91	-2.152×10^{-6}
3	235.6627	6.810 024	3.501 19	−1.171 03	-2.223×10^{-6}
4	297.6311	6.679 909	3.664 23	−1.202 19	-2.294×10^{-6}
5	357.2361	6.545 608	3.781 53	−1.733 71	-2.365×10^{-6}
6	414.4838	6.406 801	3.823 52	−3.061 90	-2.435×10^{-6}

TABLE IV. The RKR potential curve of the $B\,^1\Pi$ state. R_{min} and R_{max} are the turning points of each vibrational level. R_e is the equilibrium internuclear distance.

v	$G_v(cm^{-1})$	R_{min} (Å)	R_{max} (Å)
		$R_e = 4.0138$ Å	
−0.25	17.7537	3.8932	4.1493
0	35.4022	3.8470	4.2106
1	104.5441	3.7403	4.3791
2	171.3055	3.6733	4.5104
3	235.6627	3.6226	4.6284
4	297.6311	3.5814	4.7400
5	357.2361	3.5468	4.8484
6	414.4838	3.5169	4.9558

These results confirmed the identification of the perturbing state as $c(2)\,^3\Sigma^+$.

An e level of $^1\Pi(v',J)$, which can be excited from the $^1\Sigma^+(v'',J+1)$ level, interacts with a single $^3\Sigma^+(v,N=J,J)$ level. An f level of $^1\Pi(v',J)$, which can be excited from the $^1\Sigma^+(v'',J)$ level, interacts with both $^3\Sigma^+(v,N=J+1,J)$ and $^3\Sigma^+(v,N=J-1,J)$ levels. The non-vanishing matrix elements of the spin–orbit interaction H_{so} between the $^1\Pi$ and $^3\Sigma^+$ levels are given by[31]

$$\langle {}^1\Pi ev'JM|H_{so}|{}^3\Sigma^+ vN=JJM\rangle = \zeta/2, \tag{1}$$

$$\langle {}^1\Pi fv'JM|H_{so}|{}^3\Sigma^+ vN=J+1JM\rangle = [J/(2J+1)]^{1/2}\zeta/2, \tag{2}$$

$$\langle {}^1\Pi fv'JM|H_{so}|{}^3\Sigma^+ vN=J-1JM\rangle = [(J+1)/(2J+1)]^{1/2}\zeta/2, \tag{3}$$

If we neglect small energy terms, the rotational energies of the $^3\Sigma^+(v,N=J\ \ J+1M)$, $^3\Sigma^+(v,N=J\ \ JM)$, and $^3\Sigma^+(v,N=J\,J-1M)$ levels are degenerate, and are given by $B_vN(N+1)$. The energies of the perturbing $B\,^1\Pi(v'=4,J'=10\text{–}17)$ and $c(2)\,^3\Sigma^+(v,N=10\text{–}17)$ levels, where the vibrational quantum number v is not identified, are schematically shown in Fig. 3.

An e level $^1\Pi(ev'JM)$ interacts with a single level $^3\Sigma^+(vN=JJM)$. Hence, the perturbed level energies are expressed as

$$E_+ = \{E_2+E_1+[(E_2-E_1)^2+\zeta^2]^{1/2}\}/2, \tag{4}$$

$$E_- = \{E_2+E_1-[(E_2-E_1)^2+\zeta^2]^{1/2}\}/2, \tag{5}$$

where E_1 and E_2 are, respectively, the energies of the $B\,^1\Pi(ev'JM)$ and $c(2)\,^3\Sigma^+(vN=JJM)$ levels in the absence of the perturbation ($\zeta=0$). E_+ and E_- are, respectively, the perturbed level energies shifted toward high and low energy. The energy of the $c(2)\,^3\Sigma^+(vN=JJM)$ level at

TABLE III. Dunham coefficients and Λ doubling constants for the $B\,^1\Pi$ state of the NaK molecule. All values are given in cm^{-1} together with twice their standard deviation.

Y_{ij}		2σ
Y_{00}	16 992.753	4.40 − 03
Y_{10}	71.4381	1.18 − 02
Y_{20}	− 1.108 51	9.73 − 03
Y_{30}	− 3.0988 − 02	3.41 − 03
Y_{40}	4.6723 − 03	5.29 − 04
Y_{50}	− 2.4333 − 04	3.00 − 05
Y_{01}	7.237 09 − 02	3.28 − 06
Y_{11}	− 1.16561 − 03	5.20 − 06
Y_{21}	− 1.3723 − 05	2.18 − 06
Y_{31}	− 5.339 − 07	2.46 − 07
Y_{02}	− 2.9973 − 07	1.15 − 09
Y_{12}	− 5.151 − 09	1.94 − 09
Y_{22}	− 4.3665 − 09	8.77 − 10
Y_{32}	4.9283 − 10	1.02 − 10
Y_{03}	− 7.24 − 13	1.08 − 13
Y_{13}	− 9.806 − 13	1.92 − 13
Y_{23}	4.1654 − 13	9.54 − 14
Y_{33}	− 4.9387 − 14	1.12 − 14
y_{01}	− 2.0 − 06	2.6 − 07
y_{11}	− 0.7 − 07	0.9 − 08

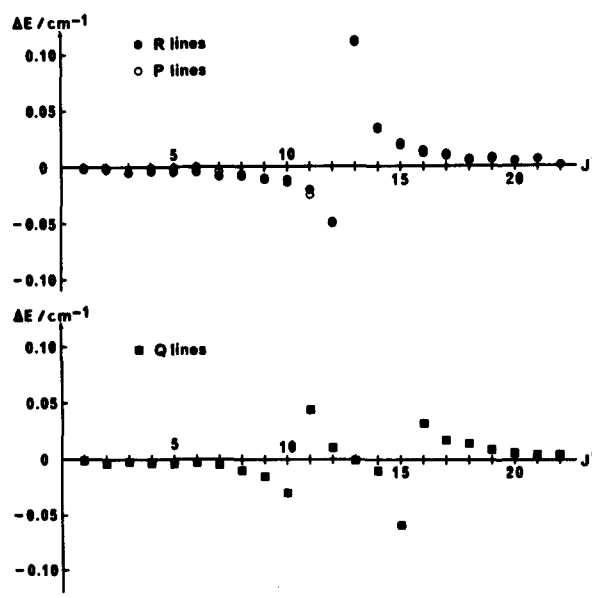

FIG. 2. Shifts of energy levels of the $B\,^1\Pi(v'=4)$ state around $J'=13$, which are determined from the difference between measured and interpolated line positions (calculated line positions using the unperturbed molecular constants listed in Table II) of the $B\,^1\Pi(v'=4)$–$X\,^1\Sigma^+(v''=1)$ transition. Upper trace for P and R lines, and lower trace for Q lines.

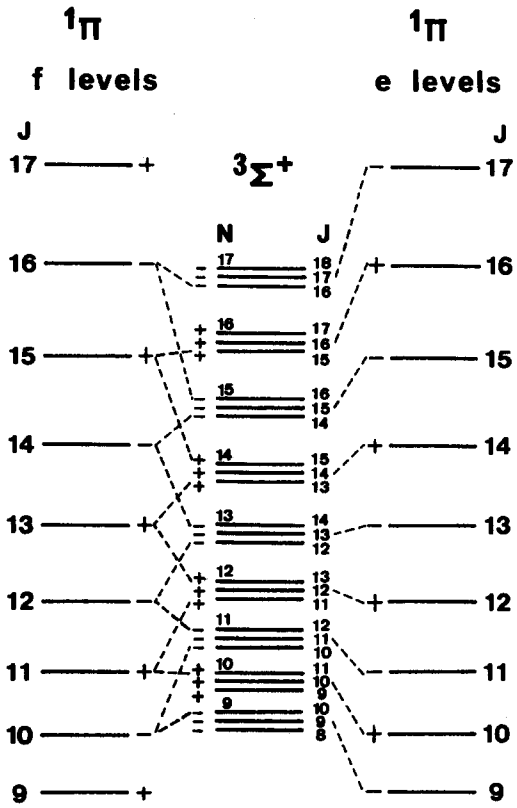

FIG. 3. Perturbing levels $B\,^1\Pi(v'=4,J'=10\text{–}17)$ and $c(2)\,^3\Sigma^+(v, N=10\text{–}17)$. The energies of the $B\,^1\Pi$ levels are calculated using the unperturbed molecular constants listed in Table II. The levels of the $c(2)\,^3\Sigma^+$ state are schematically drawn in order to explain the perturbation. The levels, which perturb each other, are connected by broken lines.

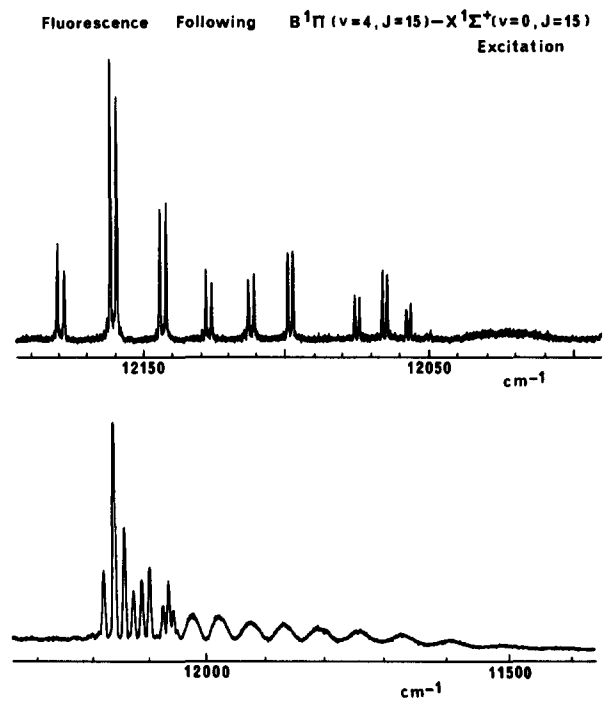

FIG. 4. Discrete and continuous parts of fluorescence to the $a(1)\,^3\Sigma^+$ state following the excitation $B\,^1\Pi(v'=4,J'=15)\leftarrow X\,^1\Sigma^+$ $(v''=0,J''=15)$. Upper trace is a high-resolution spectrum of the discrete lines. The intensity is not corrected for the intensity response of our optical system.

TABLE V. Energies of the perturbed levels $B\,^1\Pi$ $(fv=4,J)$ and $B\,^1\Pi(ev=4,J)$ calculated by assuming the unperturbed energy of the $c(2)\,^3\Sigma^+(v,N=J)$ level as $17\,293.695+0.048J(J+1)$ and $\zeta=0.28$. All values are given in cm^{-1}.

	Unperturbed level energy			
J	$c(2)\,^3\Sigma^+(vN=J)$	$B\,^1\Pi(ev=4,J)$	Perturbed energy $B\,^1\Pi(ev=4,J)$	Energy shift
17	17 308.381	17 310.760	17 310.768	+0.008
16	17 306.751	17 308.496	17 308.507	+0.011
15	17 305.215	17 306.364	17 306.381	+0.017
14	17 303.775	17 304.365	17 304.396	+0.031
13	17 302.431	17 302.499	17 302.609	+0.110
12	17 301.183	17 300.765	17 300.722	−0.043
11	17 300.031	17 299.165	17 299.143	−0.022
10	17 298.975	17 297.697	17 297.682	−0.015
9	17 298.015	17 296.362	17 296.350	−0.012
J	$c(2)\,^3\Sigma^+(vN=J)$	$B\,^1\Pi(fv=4,J)$	$B\,^1\Pi(fv=4,J)$	Shift
18	17 310.111			
17	17 308.381	17 310.759	17 310.776	+0.017
16	17 306.751	17 308.495	17 308.553	+0.058
15	17 305.215	17 306.364	17 306.345	−0.019
14	17 303.775	17 304.365	17 304.359	−0.006
13	17 302.431	17 302.498	17 302.499	+0.001
12	17 301.183	17 300.765	17 300.773	+0.008
11	17 300.031	17 299.164	17 299.204	+0.040
10	17 298.975	17 297.697	17 297.664	−0.033
9	17 298.015	17 296.362	17 296.346	−0.016
8	17 297.151			

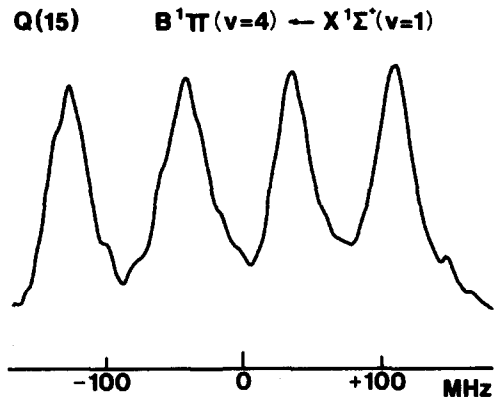

FIG. 5. High-resolution scan of the $Q(15)$ line of the $B\,^1\Pi(v'=4)$–$X\,^1\Sigma^+$ $(v''=1)$ transition. The linewidth is about 25 MHz, which is determined by the instrumental limit.

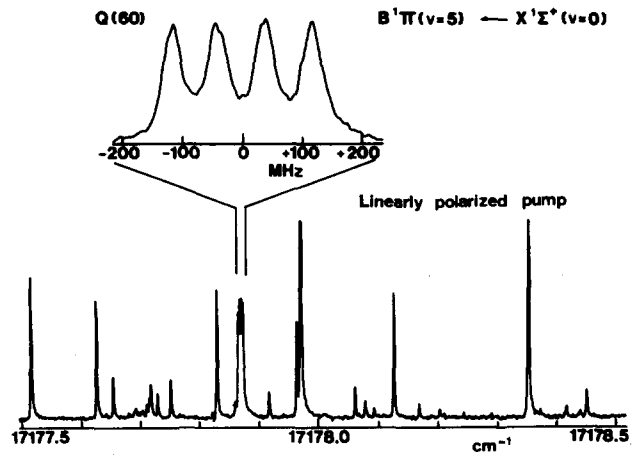

FIG. 6. A part of the laser polarization spectrum of NaK around the $B\,^1\Pi(v'=5,J'=60)$–$X\,^1\Sigma^+(v''=0,J''=60)$ transition pumped by linearly polarized light. The $Q(60)$ line is expanded. The linewidth is determined by the instrumental limit.

low J is expressed as

$$E_2 = E_v + B_v J(J+1), \tag{6}$$

where E_v is the rotationless term energy of the vibrational level v. By substituting Eq. (6) into Eqs. (4) and (5), the perturbed level energy is expressed by E_1, E_v, B_v, and ζ. We substituted the values of E_1 and E_+ or E_- for the strongly perturbed e levels $B\,^1\Pi(v'=4,J'=9$–$17)$ into either Eq. (4) or (5) depending on whether the energy shift is positive or negative. By least-squares fitting, we obtained the values $\zeta=0.28$, $B_v=0.048$, and $E_v=17\,293.695$ in units of cm^{-1}.

An f level $^1\Pi(fv'JM)$ interacts with two levels $^3\Sigma^+$ $(vN=J+1JM)$ and $^3\Sigma^+$ $(vN=J-1JM)$, and the matrix elements are given by Eqs. (2) and (3). From the constants determined above, the unperturbed energy of the $c(2)\,^3\Sigma^+(v,N=17)$ level is calculated to be lower than the energy of the $B\,^1\Pi(v'=4,J'=16)$ level, and the energy of the $c(2)\,^3\Sigma^+(v,N=16)$ level is calculated to be higher than that of the $B\,^1\Pi(v'=4,J'=15)$ level. The unperturbed energy of the $c(2)\,^3\Sigma^+(v,N=10)$ level is calculated to be lower than the energy of the $B\,^1\Pi(v'=4,J'=11)$ level, and that of the $c(2)\,^3\Sigma^+(v,N=9)$ level is calculated to be higher than the energy of the $B\,^1\Pi(v'=4,J'=10)$ level (see Table V). As shown in Fig. 2, the perturbed energy of the $B\,^1\Pi(v'=4,J'=16)$ f level is shifted toward high energy and that of the $B\,^1\Pi(v'=4,J'=15)$ f level is shifted toward low energy. The perturbed energy of the $B\,^1\Pi(v'=4,J'=11)$ f level is shifted toward high energy and that of the $B\,^1\Pi(v'=4,J'=10)$ f level is shifted toward low energy. The perturbed energy of the $B\,^1\Pi(v'=4,J')$ f level can be obtained by solving a 3×3 determinant, and the results are shown in Table V. The molecular constants of the $c(2)\,^3\Sigma^+$ state determined above also yield reasonable level energies for the shifts of the f levels (compare Fig. 2 and the energy shift in Table V).

As we can see in Fig. 1, the strongly perturbed $Q(15)$ line is broadened. Therefore, we tried to measure the line structure at the highest resolution, and we found that it was composed of four lines as shown in Fig. 5. Similar spectra were observed in other strongly perturbed Q lines. Each line was found to be composed of four lines (see Fig. 6). Both ^{23}Na and ^{39}K have nuclear spins of $I=3/2$. The splitting of the perturbed lines will be identified as the hyperfine splitting originating from the mixing of the $c(2)\,^3\Sigma^+$ and $B\,^1\Pi$ states.

The most important terms of the hyperfine interaction Hamiltonian $H_{\rm hf}$ may be the magnetic dipole interaction $H_{\rm MD}$ and the electric quadrupole interaction $H_{\rm EQ}$

$$H_{\rm hf} = H_{\rm MD} + H_{\rm EQ}. \tag{7}$$

For a diatomic molecule with nuclear spins $\mathbf{I}_1$ and $\mathbf{I}_2$, the hyperfine interaction can be written as

$$H_{\rm hf} = H_{\rm hf}(1) + H_{\rm hf}(2), \tag{8}$$

where $H_{\rm hf}(i)$ is the hyperfine interaction between the electrons and nucleus labeled i. The matrix elements of the hyperfine Hamiltonian were calculated by Broyer *et al.*[32] for homonuclear diatomic molecules. In the case of heteronuclear diatomic molecules, it is convenient to employ the coupling scheme[33]

$$\mathbf{J}+\mathbf{I}_1=\mathbf{F}_1, \quad \mathbf{F}_1+\mathbf{I}_2=\mathbf{F}_2, \tag{9}$$

where $\mathbf{J}$ is the total angular momentum excluding the nuclear spin angular momentum. The nuclear spins are coupled in order of decreasing coupling energy, and the basis functions are denoted, respectively, by $|\Lambda S\Sigma vJ\Omega I_1F_1\rangle$ for $H_{\rm hf}(1)$ and by $|\Lambda S\Sigma vJ\Omega I_1F_1I_2F_2\rangle$ for $H_{\rm hf}(2)$, where S and v are, respectively, the total electron spin and vibrational quantum numbers, Λ and Σ are, respectively, the projections of the orbital ($\mathbf{L}$) and spin ($\mathbf{S}$) angular momenta along the molecular axis. Freed[34] calculated the matrix element of $H_{\rm hf}(1)$ with the basis set $|\Lambda S\Sigma vJ\Omega I_1F_1\rangle$. The matrix element of $H_{\rm MD}(1)$ is given by

$$\langle \Lambda' S' \Sigma' v' J' \Omega' I_1' F_1' | H_{\mathrm{MD}}(1) | \Lambda S \Sigma v J \Omega I_1 F_1 \rangle$$
$$= \delta_{F_1' F_1} \delta_{I_1' I_1} F[(1)\Lambda' S' \Sigma' v' J' \Omega'; \Lambda S \Sigma v J \Omega]$$
$$\times [(2J'+1)(2J+1)(2I_1+1)I_1(I_1+1)]^{1/2} (-)^{2J'+I_1+F_1} \begin{Bmatrix} F_1 & J' & I_1 \\ 1 & I_1 & J \end{Bmatrix}, \tag{10}$$

where

$$f[(i)\Lambda' S' \Sigma' v' J' \Omega'; \Lambda S \Sigma v J \Omega] = \begin{pmatrix} J' & 1 & J \\ -\Omega' & \Delta\Omega & \Omega \end{pmatrix} \Big[\delta_{S'S} \delta_{\Sigma'\Sigma} (-)^{-\Omega'} G_{\Lambda'\Lambda}(i)$$
$$+ (-)^{-\Lambda+1+S'} \begin{pmatrix} 1 & 1 & 2 \\ \Delta\Sigma & -\Delta\Sigma-\Delta\Lambda & \Delta\Lambda \end{pmatrix} \begin{pmatrix} S' & 1 & S \\ \Sigma' & -\Delta\Sigma & -\Sigma \end{pmatrix} (30)^{1/2} D_{\Lambda'\Lambda}^{S'S}(i)$$
$$+ \delta_{\Lambda'\Lambda} (-)^{-\Lambda+\Sigma-\Sigma'+1+S'} \begin{pmatrix} S' & 1 & S \\ \Sigma' & -\Delta\Sigma & -\Sigma \end{pmatrix} K_{\Lambda'\Lambda}^{S'S}(i) \Big], \tag{11}$$

$\Delta\Sigma = \Sigma' - \Sigma, \Delta\Lambda = \Lambda' - \Lambda, \Delta\Omega = \Omega' - \Omega,$ $\begin{pmatrix} A & B & C \\ a & b & c \end{pmatrix}$ and $\begin{Bmatrix} A & B & C \\ a & b & c \end{Bmatrix}$

are, respectively, the Wigner $3-j$ and $6-j$ symbols. The matrix element of $H_{\mathrm{EQ}}(1)$ is given by

$$\langle \Lambda' S' \Sigma' v' J' \Omega' I_1' F_1' | H_{\mathrm{EQ}}(1) | \Lambda S \Sigma v J \Omega I_1 F_1 \rangle$$
$$= \delta_{F_1' F_1} \delta_{I_1' I_1} \delta_{S'S} \delta_{\Sigma'\Sigma} (-)^{-\Omega'} Q_{\Lambda'\Lambda}(i) \begin{pmatrix} J' & 2 & J \\ -\Omega' & \Delta\Omega & \Omega \end{pmatrix} [(2J'+1)(2J+1)(2I_1+3)]$$
$$\times (2I_1+2)(2I_1+1)/2I_1(2I_1-1)]^{1/2} (-)^{2J'+I_1+F_1} \begin{Bmatrix} F_1 & J' & I_1 \\ 2 & I_1 & J \end{Bmatrix}. \tag{12}$$

In these equations, $G_{\Lambda'\Lambda}(i)$ is the reduced matrix element of the interaction between the electronic angular momentum and the magnetic dipole moment of nucleus i, $D_{\Lambda'\Lambda}^{S'S}(i)$ is the reduced matrix element of the interaction between the electron spin and the magnetic moment of nucleus i, $K_{\Lambda'\Lambda}^{S'S}(i)$ is the reduced matrix element of the Fermi contact interaction, and $Q_{\Lambda'\Lambda}(i)$ is the reduced matrix element of the interaction between the nuclear quadrupole moment and the field gradient at the nucleus i. The matrix element of $H_{\mathrm{MD}}(2)$ with the basis set $|\Lambda S \Sigma v J \Omega I_1 F_1 I_2 F_2\rangle$ is given by

$$\langle \Lambda' S' \Sigma' v' J' \Omega' I_1' F_1' I_2' F_2' | H_{\mathrm{MD}}(2) | \Lambda S \Sigma v J \Omega I_1 F_1 I_2 F_2 \rangle$$
$$= \delta_{F_2' F_2} \delta_{I_2' I_2} f[(2)\Lambda' S' \Sigma' v' J' \Omega'; \Lambda S \Sigma v J \Omega] (-)^{2J'+I_1+I_2+2F_1+F_2+1}$$
$$\times [(2F_1'+1)(2F_1+1)(2J'+1)(2J+1)(2I_2+1)I_2(I_2+1)]^{1/2} \begin{Bmatrix} F_2 & I_2 & F_1' \\ 1 & F_1 & I_2 \end{Bmatrix} \begin{Bmatrix} J & F_1' & I_1 \\ F_1 & J & 1 \end{Bmatrix}. \tag{13}$$

The matrix element of $H_{\mathrm{EQ}}(2)$ can be obtained in a similar way.

If the observed hyperfine splitting is mainly due to the magnetic dipole interaction, the prominent pattern of the line splitting may be given by

$$(-)^{2J'+I_1+F_1} \begin{Bmatrix} F_1 & J' & I_1 \\ 1 & I_1 & J \end{Bmatrix}. \tag{14}$$

If it is due to the electric quadrupole interaction, the pattern of line splitting may be given by

$$(-)^{2J'+I_1+F_1} \begin{Bmatrix} F_1 & J' & I_1 \\ 2 & I_1 & J \end{Bmatrix}. \tag{15}$$

The perturbation between the $c(2)\ ^3\Sigma^+$ and $B\ ^1\Pi$ states occurs through the spin–orbit coupling, and it occurs between the same JM levels [see Eqs.(1)–(3)]. The degeneracy of the $^3\Sigma^+(v,N=JJ+1M)$, $^3\Sigma^+(v,N=JJM)$, and $^3\Sigma^+(v,N=JJ-1M)$ levels will be removed by the spin-orbit coupling. Hence, when we consider the hyperfine splitting of the perturbed lines, it will be sufficient to take into account the hyperfine interaction between the same J levels (hence $J'=J$). It is not clear at present which nuclear spin of Na and K gives the prominent hyperfine splitting, but the value of I_1 is 3/2 in either case.

For a given J and $I_1 = 3/2$, F_1 takes values of $J+3/2$, $J+1/2$, $J-1/2$, and $J-3/2$. The intensity of the hyperfine line is proportional to the degeneracy $2F_1+1$. For $J=J'=15$ and $I=3/2$, the values of Eq.(14) are -0.0674, -0.0180, 0.0284, and 0.0718, respectively, for $F_1 = 16.5$, 15.5, 14.5, and 13.5. The values of Eq.(15) are -0.0365, 0.0437, 0.0360, and -0.0443, respectively, for $F_1 = 16.5$, 15.5, 14.5, and 13.5. We shall neglect the hyperfine splitting of the $X\ ^1\Sigma^+$ state, because no hyperfine splitting has been observed in the unperturbed lines of the transitions $B\ ^1\Pi$–$X\ ^1\Sigma^+$ and $D\ ^1\Pi$–$X\ ^1\Sigma^+$. The selection rules for the electronic transition $^1\Pi$–$^1\Sigma$ are $\Delta F = \Delta J = \pm 1, 0$ and no change of the nuclear spin. Hence, $\Delta F = \Delta J = 0$ for a Q line. If the splitting is due to the magnetic dipole interaction $H_{\mathrm{MD}}(1)$, the four lines are expected to appear with the relative spacing 1.14:1.07:1.00. These values are in good agreement with the observed relative spacing 1.16:1.05:1.00 of the $Q(15)$ line of the $B\ ^1\Pi(v=4)$–$X\ ^1\Sigma^+(v=1)$ transition (See Fig. 5). If the splitting is due to the electric quadrupole interaction $H_{\mathrm{EQ}}(1)$, it will appear as almost a doublet line.

Each component of the doublet may split into a doublet by additional interaction $H_{EQ}(2)$. The resulting hyperfine lines would be composed of two doublet lines, but this is different from the observed results. The observed hyperfine splittings can be explained by the magnetic dipole interaction $H_{MD}(1)$. Furthermore, each of the four lines is expected to split into four lines by the interaction $H_{MD}(2)$ as it is expressed by Eq.(13). However, we could not observe the splitting. This shows that the splitting is small and within the resolution of our measurement; this splitting can be estimated to be less than 20 MHz. Thus, the splitting into four lines is explained by the magnetic dipole interaction due to a nucleus of $I = 3/2$.

ACKNOWLEDGMENTS

This work was supported by Grant-in-Aid for Scientific Research from the Ministry of Education (Science and Culture). H. K. thanks the Shimadzu Science Foundation for Grant-in-Aid.

[1]F. W. Loomis and M. J. Arvin, Phys. Rev. **46**, 286 (1934).
[2]M. Allegrini, L. Moi, and E. Arimondo, Chem. Phys. Lett. **45**, 245 (1977).
[3]M. M. Hessel and S. Giraud (unpublished work, 1980).
[4]J. Pfaff, M. Stock, and D. Zevgolis, Chem. Phys. Lett. **65**, 310 (1979).
[5]H. Katô and C. Noda, J. Chem. Phys. **73**, 4940 (1980).
[6]R. F. Wormsbecher, M. M. Hessel, and F. Lovas, J. Chem. Phys. **74**, 6983 (1981).
[7]C. Noda and H. Katô, Chem. Phys. Lett. **86**, 415 (1982).
[8]A. J. Ross, C. Effantin, J. D'Incan, and R. F. Barrow, J. Phys. B **19**, 1449 (1986).
[9]R. F. Barrow, R. M. Clements, G. Delacretaz, C. Effantin, J. D'Incan, A. J. Ross, J. Verges, and L. Woste, J. Phys. B **20**, 3047 (1987).
[10]R. Janoschek and H. U. Lee, Chem. Phys. Lett. **58**, 47 (1978).
[11]G. H. Jeung, J. P. Daudey, and J. P. Malrieu, Chem. Phys. Lett. **94**, 300 (1983).
[12]W. J. Stevens, D. Konowalow, and L. B. Ratcliff, J. Chem. Phys. **80**, 1215 (1984).
[13]L. B. Ratcliff and D. Konowalow, J. Mol. Spectrosc. **110**, 242 (1985).
[14]G. Igel-Mann, U. Wedig, P. Fuentealba, and H. Stoll, J. Chem. Phys. **84**, 5007 (1986).
[15]E. J. Breford and F. Engelke, Chem. Phys. Lett. **53**, 282 (1978).
[16]E. J. Breford and F. Engelke, J. Chem. Phys. **71**, 1994 (1979).
[17]D. Eisel, D. Zevgolis, and W. Demtröder, J. Chem. Phys. **71**, 2005 (1979).
[18]H. Katô and C. Noda, J. Chem. Phys. **73**, 4340 (1980).
[19]M. S. Child, H. Essen, and R. J. LeRoy, J. Chem. Phys. **78**, 6732 (1983).
[20]E. J. Breford, F. Engelke, G. Ennen, and K. H. Meiwes, Faraday Discuss. Chem. Soc. **71**, 233 (1981).
[21]J. Derouard and N. Sadeghi, J. Chem. Phys. **88**, 2891 (1987).
[22]R. F. Barrow, R. M. Clements, J. Derouard, N. Sadeghi, C. Effantin, J. D'Incan, and A. J. Ross, Can. J. Phys. **65**, 1154 (1987).
[23]W. Demtröder, *Laser Spectroscopy* (Springer, Berlin, 1982).
[24]R. N. Zare, A. L. Schmeltekopf, W. J. Harrop, and D. L. Albritton, J. Mol. Spectrosc. **46**, 37 (1973).
[25]H. Katô, M. Otani, and M. Baba, J. Chem. Phys. **89**, 653 (1988).
[26]K. Yokoyama M. Baba, and H. Katô, J. Chem. Phys. **89**, 1209 (1988).
[27]Documents of the line positions and the assignments of the NaK *B–X* band system are available on request to H. Katô.
[28]A. J. Ross, C. Effantin, J. D'Incan, and R. F. Barrow, Mol. Phys. **56**, 903 (1985).
[29]R. N. Zare, J. Chem. Phys. **40**, 1934 (1964).
[30]R. Rydberg, Z. Phys. **73**, 376 (1931); O. Klein, *ibid.* **76**, 226 (1932); A. L. G. Rees, Proc. Phys. Soc. London Ser. A **59**, 998 (1947).
[31]I. Kovacs, *Rotational Structure in the Spectra of Diatomic Molecules* (Hilger, London, 1967).
[32]M. Broyer, J. Vigue, and J. C. Lehmann, J. Phys. (Paris) **39**, 591 (1978).
[33]R. L. Cook and F. C. DeLucia, Am. J. Phys. **39**, 1433 (1971).
[34]K. F. Freed, J. Chem. Phys. **45**, 4214 (1966).